NUMEN

Determining the Nuclear Matrix Elements of Neutrinoless Double Beta Decays by Heavy-Ion Double Charge Exchange Reactions

Proponents: C. Agodi, D. Bonanno, V. Branchina, L. Calabretta, F. Cappuzzello, D. Carbone, M. Cavallaro, D.Calvo, M. Colonna, G.Cuttone, N.Desmuk, A.Ferrero, A. Foti, P. Finocchiaro, V. Greco, G. Lanzalone, F.Iazzi, R.Introzzi, A.Lavagno, D. Lo Presti, A. Muoio, L. Pandola, S.Reito, D. Rifuggiato, E. Santopinto, L.Scaltrito, G.Santagati, S. Tudisco, V.Zagatto

Spokespersons: F. Cappuzzello (cappuzzello@lns.infn.it) and C. Agodi (agodi@lns.infn.it)

Abstract: An innovative technique to access the nuclear matrix elements entering the expression of the life time of the double beta decay by relevant cross sections of double charge exchange reactions is proposed. The basic point is the coincidence of the initial and final state wave-functions in the two classes of processes and the similarity of the transition operators, which in both cases present a superposition of Fermi, Gamow-Teller and rank-two tensor components with a relevant implicit momentum transfer. First pioneering experimental results obtained at the INFN-LNS laboratory for the $^{40}Ca(^{18}O,^{18}Ne)^{40}Ar$ reaction at 270 MeV, give encouraging indication on the capability of the proposed technique to access relevant quantitative information.

A key aspect of the project is the use of the K800 Superconducting Cyclotron (CS) for the acceleration of the required high resolution and low emittance heavy-ion beams and of the MAGNEX large acceptance magnetic spectrometer for the detection of the ejectiles. The use of the high-order trajectory reconstruction technique, implemented in MAGNEX, allows to reach the high mass, angular and energy resolution required even at very low cross section. The LNS set-up is today an ideal one for this research even at a worldwide perspective. However a main limitation on the beam current delivered by the accelerator and the maximum rate accepted by the MAGNEX focal plane detector must be sensibly overcome in order to systematically provide accurate numbers to the neutrino physics community in all the studied cases. The upgrade of the LNS facilities in this view is part of this project.

Summary

Preface

The present document is divided in two parts. The first concerns with the scientific aspects and the upgrade of the detection system. This is discussed in the following. The second part deals with the technological aspects of the foreseen upgrades of the accelerator, the beam lines, the radio-protection and the associated infrastructure. This second part is presented in a specific "LNS Cyclotron Upgrade.pdf" document.

Scientific aspects

A basic question in modern physics

Neutrinoless double beta decay (*0νββ*) is potentially the best resource to probe the Majorana or Dirac nature of neutrino and to extract its effective mass. Moreover, if observed, *0νββ* will signal that the total lepton number is not conserved. Presently, this physics case is one of the most important researches "beyond the Standard Model" and might guide the way toward a Grand Unified Theory of fundamental interactions.

Since the *ββ* decay process involves transitions in atomic nuclei, nuclear structure issues must be accounted for to describe it. The $0\nu\beta\beta$ decay rate $[T_{1/2}]^{-1}$ can be factorized as a phase-space factor $G_{0\nu}$, the nuclear matrix element (NME) $M_{0\nu}$ and a term $f(m_i, U_{ei})$ containing the masses m_i and the mixing coefficients U_{ei} of the neutrino species:

$$[T_{1/2}]^{-1} = G_{0\nu}|M_{0\nu}|^2|f(m_i, U_{ei})|^2 \qquad (1)$$

where the NME is the transition amplitude from the initial φ_i to the final φ_f nuclear state of the *ββ* process through the $0\nu\beta\beta$ decay operator:

$$|M_{0\nu}|^2 = \left|\left\langle \varphi_f \left| O^{0\nu\beta\beta} \right| \varphi_i \right\rangle\right|^2 \qquad (2)$$

Thus, if the NMEs are established with sufficient precision, the neutrino masses and the mixing coefficients can be extracted from $0\nu\beta\beta$ decay rate measurements.

The evaluation of the NMEs is presently limited to state of the art model calculations based on different methods (QRPA, shell-model, IBM, EDF, etc.) [1], [2], [3], [4]. High precision experimental information from single charge exchange (CE), transfer reactions and electron capture are used to constraint the calculations [5], [6], [7], [8], [9]. However, the ambiguities in the models are still too large and the constraints too loose to reach accurate values of the NMEs. Discrepancy factors higher than two are presently reported in literature [10]. In addition some assumptions, common to the different competing calculations, could cause overall systematic uncertainties [11].

The experimental study of other nuclear transitions where the nuclear charge is changed by two units leaving the mass number unvaried, in analogy to the $\beta\beta$-decay, could give important information. Past attempts to use pion double charge exchange reactions [12], [13], [14], [15] to probe $\beta\beta$-decay NMEs were abandoned due to the large differences in the momentum transfers and in the nature of the operators [11]. Early studies of heavy-ion induced double charge exchange reactions (DCE) were also not conclusive. The reason was the lack of zero-degree data and the poor yields in the measured energy spectra and angular distributions, due to the very low cross sections involved, ranging from about 5-40 nb/sr [16], [17] to 10 µb/sr [18]. Actually, this wide range of observed cross sections has never been deeply discussed. An additional complication in the interpretation of the data was due to possible contributions of multi-nucleon transfer reactions leading to the same final states [19], [20], [21].

Here we show that the use of modern high resolution and large acceptance spectrometers allows to face the experimental challenges and to extract quantitative information from DCE reactions. The measurement of DCE high-resolution energy spectra and accurate cross sections at very forward angles is crucial to identify the transitions of interest [22]. The concurrent measurement of the other relevant reaction channels allows isolating the direct DCE mechanism from the competing transfer processes. These are at least of 4th-order and can be effectively minimized by the choice of the proper projectile-target system and incident energy [23].

DCE reactions and 0νββ decays

The availability for the first time of valuable data on DCE reactions raises the question whether they can be used toward the experimental access to $0\nu\beta\beta$ NMEs. Although the DCE and $0\nu\beta\beta$ decay processes are mediated by different interactions, there are a number of important similarities among them:

1.   Parent/daughter states of the $0\nu\beta\beta$ decay are the same as those of the target/residual nuclei in the DCE;

2. Short-range Fermi, Gamow-Teller and rank-2 tensor components are present in both the transition operators, with relative weight depending on incident energy in DCE;

3. A large linear momentum (~100 MeV/c) is available in the virtual intermediate channel in both processes [10]. This is a crucial similarity since other processes cannot probe this feature [24];

4. The two processes are non-local and are characterized by two vertices localized in a pair of valence nucleons;

5. Both processes take place in the same nuclear medium. In medium effects are expected to be present in both cases, so DCE data could give a valuable constraint on the theoretical determination of quenching phenomena on $0\nu\beta\beta$. One should mention for example that in single β-decay, $2\nu\beta\beta$-decay [4] and charge exchange reactions [25], the limited model space used in the calculations and the contribution of non-nucleonic degrees of freedom and other correlations require a renormalization of the coupling constants in the spin-isospin channel. However an accurate description of quenching has not yet been fully established and other aspects of the problem can give important contributions [26];

6. An off-shell propagation through virtual intermediate channels is present in the two cases. The virtual states do not represent the asymptotic channels of the reaction and their energies can be different from those (measurable) at stationary conditions [27]. In practice, a supplementary contribution of several MeV to the line width is present in the intermediate virtual states. This is related to the transit time of a particle (neutrino in one case and pair of nucleons in the other) along the distance of the two vertices of the $0\nu\beta\beta$ and DCE processes. The situation is very different in CE reactions, where the intermediate states of $0\nu\beta\beta$ are populated as stationary ones and in $2\nu\beta\beta$, where the neutrinos and electrons are projected out from the nucleus. No effective broadening of the line width is thus probed in CE and $2\nu\beta\beta$.

The descriptions of NMEs for DCE and $0\nu\beta\beta$ present the same degree of complexity, with the advantage for DCE to be "accessible" in laboratory. However, a simple relation between DCE cross sections and $\beta\beta$-decay half-lives is not trivial and needs to be explored.

Factorization of DCE cross section

It is well known that single β-decay strengths are proportional to CE reaction cross sections for linear momentum transfer $q \sim 0$ and under specific conditions [25], [28], [29], [30], [31]:

$$\frac{d\sigma}{d\Omega}(q,E_x) = \hat{\sigma}_\alpha(E_p,A)F_\alpha(q,E_x)B_T(\alpha)B_P(\alpha) \qquad (3)$$

where $B_T(\alpha)$ and $B_P(\alpha)$ are the target and projectile β-decay reduced transition strengths (related to the matrix elements $M(\alpha)$[1]) for the $\alpha =$ Fermi (F) or Gamow-Teller (GT) operators[2]. The factor $F_\alpha(q,E_x)$ describes the shape of the cross section distribution as a function of the linear momentum transfer q and the excitation energy E_x. For $L = 0$ transitions, it depends on the square of the $j_0(qr)$ spherical Bessel function [29], [25]. The quantity $\hat{\sigma}_\alpha$, named "unit cross section", is of primary interest since it almost behaves as a universal property of the nuclear response to F and GT probes. The dependence on the projectile energy E_p and on the target mass number A is in fact quite smooth and computable all along the nuclear chart. In a rigorous Distorted Wave approach as that proposed by Taddeucci et al. [29], the unit cross section for a CE process is factorized as:

$$\hat{\sigma}(E_p,A) = K(E_p,0)|J_\alpha|^2 N_\alpha^D \qquad (4)$$

where $K(E_p,E_x)$ is a kinematic factor, J_α is the volume integral of the effective isovector nucleon-nucleon interaction and N_α^D expresses the distortion of the incoming and outcoming waves in the scattering [31].

Eqs. (3)-(4) are routinely used for accurate (within few percent) determination of the strengths B in light-ion induced reactions such as (n,p), (p,n), (^{3}He,t), (t,^{3}He), (d,^{2}He) at bombarding energies above 100 AMeV [32], [24], [33], [34]. For heavy-ion induced reactions, the data analyses are typically more involved, due to the projectile degrees of freedom and the sizeable amount of momentum transfer. A relevant simplification comes from the strong absorption of the scattering waves in the inner part of the colliding systems and the resulting surface localization of such reactions. As a consequence in these cases, the use of fully consistent microscopic approaches with double folded potentials for the reaction form factors still allows the determination of $B(\alpha)$ within 10-20% [35].

Under the hypothesis of a surface localized process, a generalized version of eq. (3) is assumed also for DCE within a similar distorted wave approach:

----

[1] In this document $B(\alpha) = \frac{1}{2J_i+1}|M(\alpha)|^2$, where J_i is the angular momentum of the initial state.

[2] Usually for (p,n) and (n,p) reactions the $B_P(\alpha)$ strength does not explicitly appear in the formula and is included in $\hat{\sigma}_\alpha(E_p,A)$. In this paper, following this convention, $B_P(\alpha)$ in eq. (3) is divided by the $B_P(\alpha)$ related to the (p,n), which is 3.049 [32].

$$\frac{d\sigma^{DCE}}{d\Omega}(q,E_x) = \hat{\sigma}_\alpha^{DCE}(E_p,A)F_\alpha^{DCE}(q,E_x)B_T^{DCE}(\alpha)B_P^{DCE}(\alpha) \qquad (5)$$

where the superscripts indicate that the factors refer to the DCE process. The $B_{T,P}^{DCE}(\alpha)$ are connected to the nuclear matrix elements of the $\beta\beta$-decay. In analogy to the CE, the q dependence of the cross section is given by a Bessel function. A DCE unit cross section can be defined as follows:

$$\hat{\sigma}_\alpha^{DCE}(E_p,A) = K(E_p,0)\left|J_\alpha^{DCE}\right|^2 N_\alpha^D \qquad (6)$$

where $K(E_p,0)$ and N_α^D are the same as in eq. (4) and J_α^{DCE} is the volume integral of the double charge exchange interaction. A closer inspection of eqs. (4) and (6) reveals that the specificity of the single or double charge exchange unit cross sections is expressed through the volume integrals of the potentials, while the other factors are general features of the scattering. A model for the two-vertex interaction is needed to extract physical information from measured DCE cross sections. At the present time, a complete and coherent theory of such an interaction does not exist to the best of our knowledge. In a simple model, one can assume that the DCE process is just a second order charge exchange, where projectile and target exchange two uncorrelated isovector virtual mesons. The transition from initial $|i\rangle$ to final $|f\rangle$ reaction channels proceeds via the intermediate channels $|n\rangle$. Here the term channel is used to refer to a particular internal state of a partition in a particular state of relative motion [36]. This gives rise to a *VGV*-like term in the volume integral $\left|J_\alpha^{DCE}\right|^2$ which describes the action of the interaction V in two vertices. As pointed out in ref. [19], for DCE it has a non-vanishing contribution in a region around the overlapping surfaces of the colliding nuclei. The propagator is

$$G = \sum_n \frac{|n\rangle\langle n|}{E_n - (E_i + E_f)/2} \qquad (7)$$

where $E_{i,n,f}$ indicate the energies of the initial, intermediate and final channels, respectively. The explicit coordinate representation of G, which accounts for the relative motion in $|n\rangle$ is given in ref. [36]. In eq. (7), E_n is a complex number whose imaginary component represents the off-shell

propagation through the virtual intermediate states. This approach is analogous to the double-phonon model in giant resonance studies [37].

The NUMEN goals

Studying if the unit cross section is a smooth and thus controllable function of E_p and A is the first and most ambitious goal of our project. If achieved, this result will provide an experimental approach to $0\nu\beta\beta$ decay nuclear matrix elements. This corresponds to verify that Eqs.(5-6) give an accurate description of the reaction mechanism, factorized in a reaction part and a nuclear structure part, this latter factorized in a projectile and target matrix element. The development of a consistent microscopic description of the heavy-ion double charge exchange reaction and the nuclear structure part is essential to this purpose. The use of the quantum approach for the DWBA or CRC cross section with form factors including QRPA transition densities (as well as Shell Model or IBM densities) is a suitable framework in which this theory can be developed. Experimentally the achievement of the first goal requires that a systematic set of appropriate data is built, facing the relative experimental challenges connected with the low cross sections and high resolutions requests.

Moreover the project has two other goals, ground-breaking and achievable in a shorter period. The measured DCE absolute cross sections provide themselves a powerful tool for tuning the nuclear structure theory. The matrix elements for double charge exchange and neutrino-less double beta decay probe the same initial and final wave functions by operators with similar structure. Consequently the measured DCE absolute cross sections allows to test the goodness of the assumptions done for the unavoidable truncation of the many-body wave functions. The reaction part need to be precisely controlled to this purpose, a result that is at reach within a fully quantum scattering framework. Once the nuclear wave functions have been tested by DCE cross sections, the same can be used for $0\nu\beta\beta$ decay nuclear matrix elements. Promoting the development of these kind of constrained theories for the NME of the neutrino-less double beta decay is thus an important goal that NUMEN can achieve even with a reduced experimental dataset and without assuming cross section factorization.

Finally the third goal is to provide relative NME information on the "hot cases" of the $0\nu\beta\beta$ decay. In case of validity of cross section factorization, the ratio of measured cross sections can give a model independent way to compare the sensitivity of different half-life experiments. This result can be achieved even in presence of sizeable systematic errors in the measured cross sections and in the extraction of unit cross sections, as they are largely reduced in the ratio. Performing these comparative analyses could strongly impact in the future developments of the field, especially in a scenario were fundamental choices for the best isotope candidates for $0\nu\beta\beta$ decay need to be done.

Phase 1: the pilot experiment

The ^{40}Ca(^{18}O,^{18}Ne)^{40}Ar DCE reaction has been measured at the INFN-LNS laboratory in Catania together with the competing processes: ^{40}Ca(^{18}O,^{18}F)^{40}K single charge exchange, ^{40}Ca(^{18}O,^{20}Ne)^{38}Ar two-proton (2p) transfer and ^{40}Ca(^{18}O,^{16}O)^{42}Ca two-neutron (2n) transfer. A beam of ^{18}O^{4+} ions, extracted by the K800 Superconducting Cyclotron accelerator, bombarded a 279±30 μg/cm^2 Ca target, at 270 MeV incident energy. A total charge of 3.6 mC was integrated by a Faraday cup, downstream the target. The ejectiles produced in the collisions were momentum-analysed by the MAGNEX large acceptance spectrometer [38] and detected by its focal plane detector [39], [40]. An angular range of -1.2° < θ_{lab} < +8° in the laboratory frame was explored, corresponding to scattering angles in the center of mass 0° < θ_{CM} < 12°. The ejectiles identification was achieved as described in refs. [41], [42]. The positions and angles of the selected ions measured at the focal plane were used as input for a 10th order ray-reconstruction of the scattering angle θ_{CM} and excitation energy $E_x = Q_0 - Q$ (where Q_0 is the ground-to-ground state reaction Q-value) [43], [44], [45]. Figure 1 shows examples of the measured energy spectra. An energy resolution of ~500 keV (full width at half maximum) is obtained similarly to ref. [46]. The absolute cross section was extracted from measured yields according to ref. [43]. A systematic error of ~20% was estimated from the uncertainty in the target thickness and beam collection.

Experimental results

In the ^{40}Ca(^{18}O,^{20}Ne)^{38}Ar 2p-transfer energy spectrum of Figure 1a, the cross section tends to increase with excitation energy as a consequence of the kinematical Q-matching conditions (Q_{opt} = 32 MeV). Known low-lying states are identified indicating the suppression of low multipolarity transitions due to L-matching conditions (L_{opt} = 6). The L- and Q-optimum for the second step 2n-transfer ^{38}Ar(^{20}Ne,^{18}Ne)^{40}Ar are similar. Thus multistep transfer reactions are expected to be strongly suppressed in the population of the mismatched (L = 0, Q = -2.9 MeV) ^{40}Ar ground state. In addition, the required condition of a 2n-transfer from the high spin intermediate states populated in the ^{40}Ca(^{18}O,^{20}Ne)^{38}Ar to the 0$^+$ ^{40}Ar$_{g.s.}$ gives a supplementary reduction due to the vanishing Clebsh-Gordan coefficients. The cross section around zero-degree is ~3 μb/sr for the ^{40}Ca(^{18}O,^{20}Ne)^{38}Ar$_{gs}$, not larger than the ^{40}Ca(^{18}O,^{18}Ne)^{40}Ar$_{gs}$ (~ 11 μb/sr). This is very different from what reported in ^{14}C + ^{40}Ca at 51 MeV where the ^{40}Ca(^{14}C,^{16}O)^{38}Ar 2p-transfer cross section is ~1 mb/sr, i.e. almost two orders of magnitude larger than the corresponding ^{40}Ca(^{14}C,^{14}O)^{40}Ar DCE [18]. Bes et al. [19] and Dasso and Vitturi [20] conclude that the ^{14}C + ^{40}Ca → ^{16}O + ^{38}Ar → ^{14}O$_{gs}$ + ^{40}Ar$_{gs}$ transfer route is the leading mechanism feeding the ^{40}Ar$_{gs}$. The reason is the much better

matching of the 2p-transfer in the ^{14}C + ^{40}Ca (Q_{opt} = 10 MeV, L_{opt} = 3) compared to our case. Assuming a similar scaling between 2p-transfer and DCE for the present data, an upper limit of 30 nb/sr in the (^{18}O,^{18}Ne) reaction channel is estimated for the ^{18}O + ^{40}Ca → ^{20}Ne + ^{38}Ar → ^{18}Ne$_{gs}$ + ^{40}Ar$_{gs}$ multi-step route. Even considering the coherent sum of DCE and transfer amplitudes, a contribution of less than 10% is found at zero-degree.

The 2n-pickup 2p-stripping channel ^{18}O + ^{40}Ca → ^{16}O + ^{42}Ca → ^{18}Ne$_{gs}$ + ^{40}Ar$_{gs}$ is unlikely to contribute significantly, since the first step is already very suppressed in our experiments, with cross sections which are about half the cross section of the 2p-transfer.

The ^{40}Ca(^{18}O,^{18}F)^{40}K single charge exchange spectrum is shown in Figure 1b. Some structures is observed below 5 MeV excitation energy, however the limited resolution and the high level density do not allow to isolate single transitions. The strongest group is between 500 keV and 1.2 MeV where the transitions to the known 2$^-$ and 5$^-$ states of ^{40}K at 800 and 892 keV and those to the excited states of the ^{18}F ejectiles at 937, 1041, 1080 and 1121 keV, if populated, are not resolved [47], [48]. In particular, the dominance of the excited states of ^{18}F at 1041, 1080 and 1121 keV is ruled out by a least square analysis, considering that they will generate Doppler broadened peaks with an extra width of about 300 keV. A number of ^{40}K states are known in the region between 1.8 and 2.8 MeV. Calculations based on the Quasi Particle Random Phase Approximation – Distorted Wave Born Approach of ref. [35] indicate that the cross-section is mainly distributed among the 4$^-$, 2$^-$, 1$^+$ and 3$^-$ transitions. In particular the 1$^+$ accounts for about 40 μb/sr, consistent with the 38 μb/sr extracted from eqs. (3)-(4) using the parameters values reported in Section 6.1. A more detailed analysis of the single charge exchange reaction is beyond the scope of the present letter and will be published elsewhere.

In the DCE energy spectrum of Figure 1c, the ^{40}Ar ground state is clearly separated from the not resolved doublet of states ^{40}Ar 2$^+$ at 1.460 MeV and ^{18}Ne 2$^+$ at 1.887 MeV. At higher excitation energy the measured yield is spread over many overlapping states. The angular distribution for the transition to the ^{40}Ar 0$^+$ ground state is shown in Figure 2. A clear oscillating pattern is observed. The position of the minima is well described by a $|j_0(qR)|^2$ Bessel function, where R = 1.4 ($A_1^{1/3}$+$A_2^{1/3}$) and $A_{1,2}$ is the mass number of projectile and target. Such an oscillating pattern is not expected in complex multistep transfer reactions, due to the large number of angular momenta involved in the intermediate channels, which would determine a structure-less cross section slowly decreasing at larger angles. The experimental slope is shallower than the Bessel function as expected since a plane-wave description is not appropriate [36]. Despite that, a very simple model of L = 0 direct process reasonably well describes the main features of the experimental angular distribution.
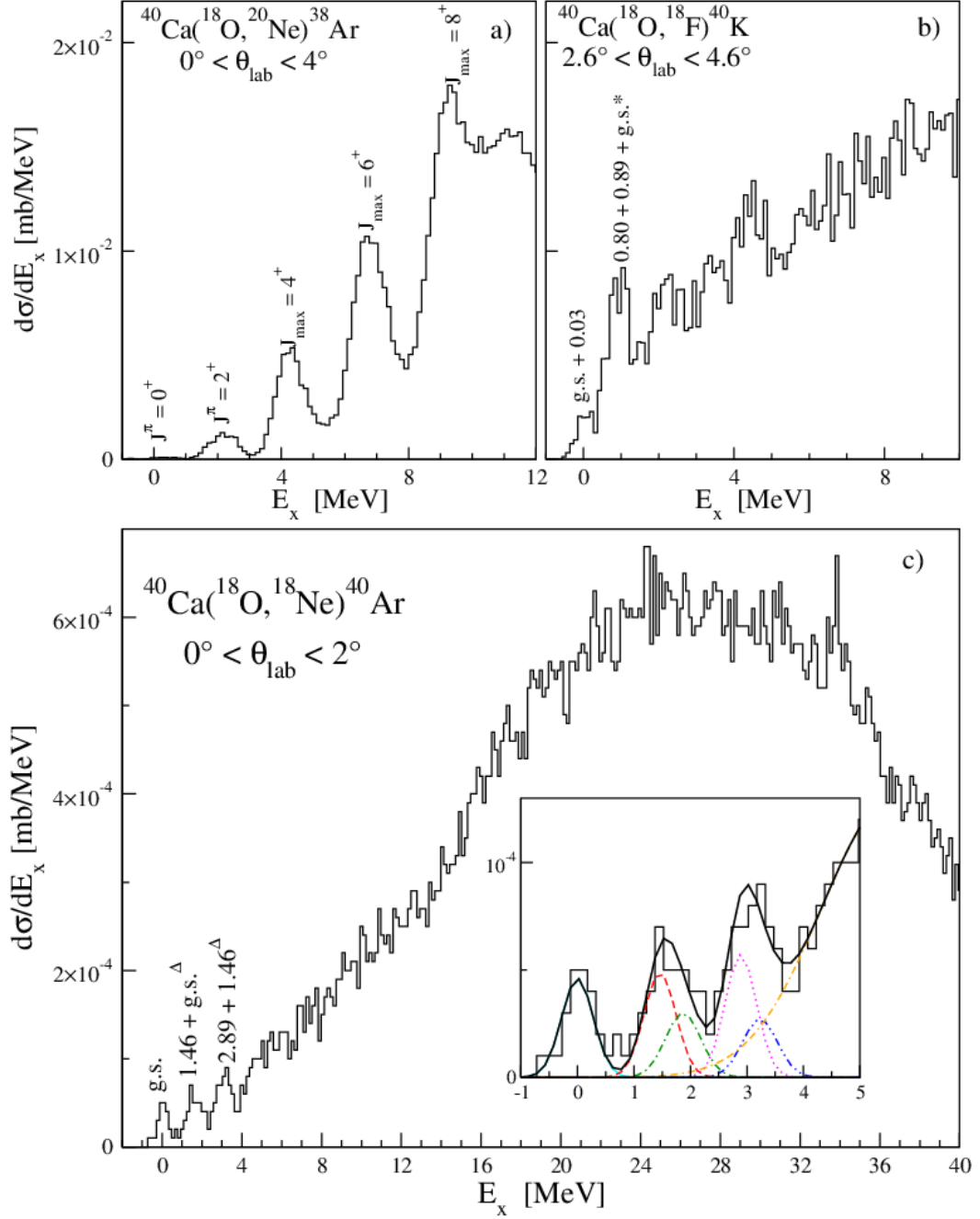
Figure 1. (a) Energy spectrum measured in the $^{40}Ca(^{18}O,^{20}Ne)^{38}Ar$ 2p-transfer. Above 3 MeV excitation energy, different states are overlapped in the observed peaks and the maximum angular momentum (J_{max}) is indicated according to [49]. (b) Energy spectrum from $^{40}Ca(^{18}O,^{18}F)^{40}K$ single charge exchange. The symbol g.s.* indicates the $^{40}Ca(^{18}O,^{18}F_{0.937MeV})^{40}K_{g.s.}$ transition. (c) Energy spectrum from $^{40}Ca(^{18}O,^{18}Ne)^{40}Ar$ DCE. The symbols g.s.$^\Delta$ and 1.46$^\Delta$ indicate the $^{40}Ca(^{18}O,^{18}Ne_{1.87MeV})^{40}Ar_{g.s.}$ and $^{40}Ca(^{18}O,^{18}Ne_{1.87MeV})^{40}Ar_{1.46MeV}$ transitions, respectively. In the insert, a zoomed view of the low-lying states and, superimposed (black solid line), a fit with 6 Gaussian functions are shown. They are centered at 0 (cyan solid), 1.46 (red dashed), 1.87 (green dot-dashed), 2.89 (magenta dotted), (1.46 + 1.87) = 3.33 (blue double dot-dashed), 5.6 MeV (orange dot-double dashed). The widths are given by the experimental resolution plus the Doppler

broadening, except for the 5.6 MeV Gaussian whose width is 3 MeV. In (b) and (c) the symbol + indicates the presence of unresolved states.
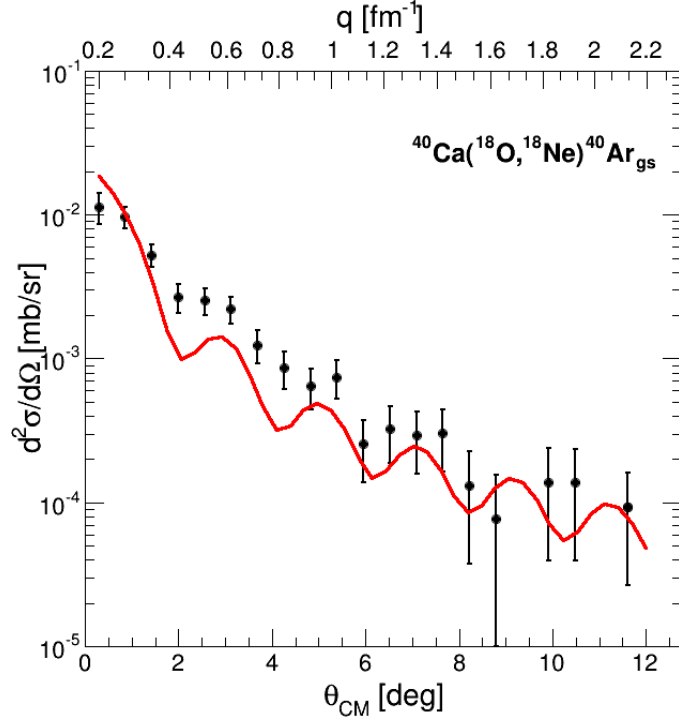
Figure 2. Differential cross section of the $^{40}Ca(^{18}O,^{18}Ne)^{40}Ar_{g.s.}$ transition as a function of θ_{CM} and q. The error bars include a statistical contribution and a component due to the solid angle determination. The red curve represents the L = 0 Bessel function folded with the experimental angular resolution (~ 0.6°) and scaled to reproduce the incoherent sum of the predicted double F and GT cross sections (see text).

Cross section analysis

In order to check the validity of the factorization in eqs. (5)-(6) we deduce the unit cross section and the matrix element for the DCE process assuming either a pure double *GT* or *F* transition.

Gamow-Teller

As discussed in Section 3, the J_{GT}^{DCE} volume integral for the ^{18}O + ^{40}Ca $\rightarrow$ ^{18}F$_{gs}$(1^+) + ^{40}K$_{0\text{-}8\text{MeV}}$(1^+) $\rightarrow$ ^{18}Ne$_{gs}$ + ^{40}Ar$_{gs}$ at 270 MeV incident energy is estimated starting from the CE volume integral. We get J_{GT} = 231 MeV·fm^3 using the isovector parts of the D3Y G-matrix [50], which includes spin-dependent and spin-independent direct and exchange central interactions. This is known to be an adequate choice at the energy of the present experiment, as described in [35]. The G propagator of eq. (7) is calculated summing over the on-shell energy distribution of ^{40}K 1^+ states observed in high resolution (^{3}He,t) data on ^{40}Ca target [51] and on ^{18}F 1^+ ground state, as sketched in Figure 3. The off-shell contribution to G, accounting for ~7 MeV (full width at half maximum), is estimated from the crossing time ($\Delta t \sim 27$ fm/c) of the two pairs of nucleons participating in the DCE at 15 AMeV, assuming a correlation length of 4.8 fm from ref. [52].

A distortion factor $N_\alpha^D \sim 0.042$ is calculated as the ratio of Distorted Wave over Plane Wave CE cross sections using the double folded optical potential of ref. [35]. Taking into account the kinematic factor $K \sim 0.0089$ [29], a $\hat{\sigma}_{GT}^{DCE} \sim 76$ µb/sr is estimated for the ^{40}Ca(^{18}O,^{18}Ne)^{40}Ar DCE reaction at $q = 0$ from eq. (6). The correction factor of eq. (5) for $q = 0.18$ fm^{-1}, corresponding to $\theta_{CM} \sim 0°$ (measured angular interval $0° < \theta_{CM} < 0.6°$) is $F_{GT}^{DCE} \sim 0.72$. From the measured $\frac{d\sigma^{DCE}}{d\Omega}$ ($\theta_{CM} = 0°$) = 11 µb/sr, one obtains an estimation of the maximum strength from eq. (5)

$$B^{DCE}(2GT) = B_T^{DCE}(2GT) \cdot B_P^{DCE}(2GT) = \frac{\frac{d\sigma^{DCE}}{d\Omega}(q,E_x)}{\hat{\sigma}_{GT}^{DCE}(E_p,A) F_{GT}^{DCE}(q,E_x)} \leq 0.20. \tag{8}$$

This is compared to the value obtained combining the strengths, taken from literature, for the transitions in the projectile and target sketched in Figure 3 and listed in Table 1

$$B(2GT) = B_P(2GT) \cdot B_T(2GT) = 0.11 \tag{9}$$

Here the B transition strengths reduced for spin and isospin according to ref. [32] are used. In particular, for the projectile we have

$$B_P(2GT) = B[GT;{}^{18}O_{gs}(0^+) \rightarrow {}^{18}F_{gs}(1^+)] \cdot B[GT;{}^{18}F_{gs}(1^+) \rightarrow {}^{18}Ne_{gs}(0^+)] = 1.14 \tag{10}$$

13

where only the population of the $^{18}F_{g.s.}$ is taken into account, as found in ref. [53] and the $B(GT)$ for the second step is from [54]. These factors are listed in table 1.

For the target

$$B_T(2GT) = \sum (B[GT;{}^{40}Ca_{gs}(0^+) \rightarrow {}^{40}K(1^+)] \cdot B[GT;{}^{40}K(1^+) \rightarrow {}^{40}Ar_{gs}(0^+)]) = 0.095 \qquad (11)$$

where the sum refers to the transitions to the ^{40}K 1^+ states up to 8 MeV observed in ref. [55]. The $B[GT;{}^{40}K(1^+) \rightarrow {}^{40}Ar_{gs}(0^+)]$ are taken from ref. [55]. For the $^{40}Ca_{gs}(0^+) \rightarrow {}^{40}K(1^+)$ transitions, we use high resolution $^{40}Ca(^3He,t)^{40}Sc$ data not yet published from Fujita et al. [51], assuming isospin symmetry. These data were also compared to previous results taken from literature: the $^{40}Ca(p,n)^{40}Sc$ reaction at 159 MeV from [28] and at 134 MeV from [56]. In ref. [28] Taddeucci et al. give zero-degree cross section 1.2 mb/sr and a value of $B(GT; 2.73$ MeV$) = 0.21 \pm 0.04$ for the transition to the strongest 1^+ state of ^{40}K at 2.73 MeV. These results conflict with Chittrakarn et al. [56] who measure a zero-degree cross section of 0.48 mb/sr for the same state, from which one can extract $B(GT; 2.73$ MeV$) \sim 0.084$. In addition we also considered the results of Park et al. [57] who extract $B(GT; 2.73$ MeV$) = 0.14 \pm 0.02$ from multiple decomposition analysis of the zero-degree cross section of the $^{40}Ca(n,p)^{40}K$ reaction at 170 MeV. However, the results of Park et al. could be influenced by large systematic errors, due to the poor energy resolution and the uncertainties of the multiple decomposition analysis.

Preliminary results from the high resolution experiment of Fujita et al. [51] confirm the results of Chittrakarn et al. and this gives us confidence about the results from zero-degree cross section of the $(^3He,t)$ reaction. In addition the $(^3He,t)$ experiment also shows that, apart the 1^+ state at 2.73 MeV, which carries a strength of $B(GT; 2.73$ MeV$) = 0.069 \pm 0.006$, the GT strength is fragmented in other 10 satellites. The two largest ones are at 2.33 and 4.40 MeV, which account for $B(GT; 2.33$ MeV$) = 0.014 \pm 0.001$ and $B(GT; 4.40$ MeV$) = 0.018 \pm 0.002$, respectively.

Only the 2.33, 2.73 and 4.40 MeV 1^+ states of ^{40}K give a not negligible contribution to the eq. (11). Merging the $B(GT)$ values from [55] and [51], we get the sum given in eq. (11). The total results and the partial numbers used to get this estimation are listed in Table 1.

The small value of $B^{DCE}(2GT)$ and $B(2GT)$ for the ^{40}Ca is a consequence of the Pauli blocking in this doubly magic system. The GT transitions take place only through the small $1f_{7/2}$, $1f_{5/2}$ particle and $1d_{3/2}$ hole components of the $^{40}Ca_{g.s.}$ wave function, which account for about 14% of the total [58], [59].

14
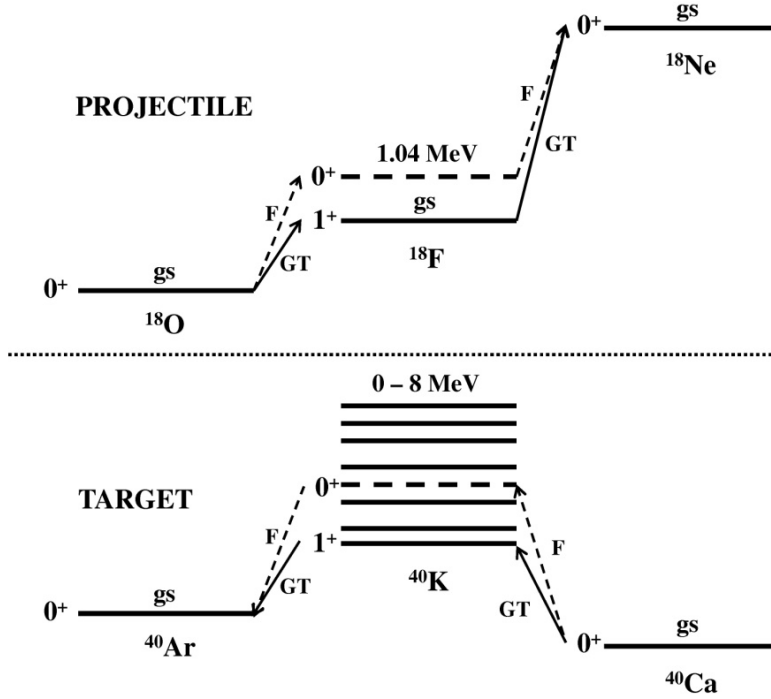
Figure 3. Diagram for the *GT* and *F* projectile and target transitions used for the determination of the *B*(2*GT*) and *B*(2*F*). See text.

Fermi

A similar procedure was applied assuming a pure double Fermi operator for the DCE to the $^{40}\text{Ar}_{gs}$. At the present energy the CE volume integral is $J_F = 253$ MeV·fm^3, very close to the *GT* case. Only the ^{40}K 0^+ state at 4.38 MeV and the ^{18}F 0^+ state at 1.04 MeV are considered in the intermediate channel. By the same arguments of the *GT* case, we obtain $\hat{\sigma}_F^{DCE} \sim 46$ μb/sr from eq. (6) and $F_F^{DCE} \sim 0.77$ at $\theta_{CM} \sim 0°$. As a consequence

$$B^{DCE}(2F) = B_T^{DCE}(2F) \cdot B_P^{DCE}(2F) = \frac{\frac{d\sigma^{DCE}}{d\Omega}(q,E_x)}{\hat{\sigma}_F^{DCE}(E_p,A)F_F^{DCE}(q,E_x)} \leq 0.31. \tag{12}$$

This value is close to the product of the known *B*(*F*) for the transitions in the projectile and target through the 1.04 MeV and 4.38 MeV 0^+ states of ^{18}F and ^{40}K, respectively (see Fig. 3):

15

$$B(2F) = B_P(2F) \cdot B_T(2F) = 0.42 \tag{13}$$

Here $B_P(2F) = 4$ is taken from the Fermi sum rule. $B_T(2F) = 0.053 \cdot 2$ is extracted by [55] and [51].

Table 1: Extracted strengths for pure Fermi and pure Gamow-Teller transitions and comparison with literature.

	$B_{DCE}(2\alpha)$ this work	$B(2\alpha)$ literature	B_P ($^{18}O \to ^{18}F$)	B_P ($^{18}F \to ^{18}Ne$)	$B_P(2\alpha)$	$E(^{40}K)$ MeV	B_T ($^{40}Ca \to ^{40}K$)	B_T ($^{40}K \to ^{40}Ar$)	$B_T(2\alpha)$
						2.33	0.014 [c]	1.03 [d]	
						2.73	0.069 [c]	0.95 [d]	
T	0.20	0.11	1.07 [a]	1.05 [b]	1.14	4.40	0.018 [c]	0.54 [d]	0.095
						4.50-8	8*0.007 [c]	0.10 [d]	
	0.31	0.42	2	2	4		0.053 [c]	2	0.106

a) From ref. [53], divided by $B_{(p,n)}(GT) = 3.049$
b) From ref. [54], divided by $B_{(p,n)}(GT) = 3.049$
c) From ref. [51]
d) From ref. [55]

DCE nuclear matrix elements

Under the hypothesis of pure *GT* transition, $B_T^{DCE}(2GT)$ can be extracted dividing eq. (8) by $B_P^{DCE}(2GT)$, assuming $B_P^{DCE}(2GT) = B_P(2GT) = 1.14$ (see eq. (10)). The NME can be then derived from $B_T^{DCE}(GT)$ via

$$\left| M_T^{DCE}(\alpha) \right|^2 = B_T^{DCE}(\alpha) \tag{14}$$

obtaining $M_T^{DCE}(GT) = 0.42 \pm 0.21$. In the lack of theoretical predictions for the [40]Ca NME, it is worth to compare this value with the well-studied [48]Ca NME, which ranges from 0.67 [1] to 1.53 [4] depending on different models. The smaller value obtained for [40]Ca is compatible with the effect of Pauli blocking present only in this system, which determines reduction of a factor about 7 for F and GT.

Analogously, in the case of pure Fermi process, we extract $M_T^{DCE}(F) = 0.28 \pm 0.14$ from eqs. (12-14). The uncertainty in the determination of M_T^{DCE} is about ±50%, estimated by checking the sensitivity of the results to the used parameters.

Both *F* and *GT* contribute to the total cross section at $\theta_{CM} = 0°$. Their size can be predicted by $B(2GT) \cdot \widehat{\sigma}_{GT}^{DCE} \cdot F_{GT}^{DCE} \sim 6$ μb/sr for Gamow-Teller and $B(2F) \cdot \widehat{\sigma}_F^{DCE} \cdot F_F^{DCE} \sim 15$ μb/sr for Fermi. The comparison is much more accurate than the single estimation due to the common assumptions done. The *L* = 0 Bessel function shown in Figure 2 is scaled to give a cross section of 21 μb/sr at $\theta_{CM} = 0°$, which is the incoherent sum of the predicted *GT* and *F* cross sections. The comparison with the experimental data show a remarkable quantitative agreement. However, the effects of the interference should be studied in detail. The fact that both pure *GT*- and *F*-like extreme models give comparable contributions to the final cross section is a direct consequence of the similar volume integrals for both operators. The relation between these volume integrals resembles that for nucleon-nucleon interaction at 15 MeV. This indicates that the reaction mechanism is largely determined by the effective nucleon-nucleon interaction. Experiments at different incident energies are envisaged in order to explore conditions characterized by different weights of *GT*-like and *F*-like contributions and disentangle the role of each operator. In particular, higher energies are more suitable to study the *GT*-like NMEs, which are expected to be dominant in most of the *0νββ* decays.

0νββ nuclear matrix elements

In the previous sections we showed that in the extreme hypothesis of pure Gamow-Teller or Fermi transition the extracted matrix elements are $M_T^{DCE}(GT) = 0.42 \pm 0.21$ or $M_T^{DCE}(F) = 0.28 \pm 0.14$, respectively. We notice that they are very similar, so even the weighted average, representing a more realistic combination of both contribution, will be. Assuming the known *GT* and *F* strengths from literature (see discussion section 6.3) we can get an estimate of the weights through the expression of the DCE cross section expected at zero-degree:

$$\frac{d\sigma}{d\Omega}(\theta = 0°, E_x = 0) = \widehat{\sigma}_{GT}^{DCE}\, F_{GT}^{DCE}\, B(2GT) + \widehat{\sigma}_F^{DCE}\, F_F^{DCE}\, B(2F) = 6\frac{\mu b}{sr} + 15\,\frac{\mu b}{sr} = 21\frac{\mu b}{sr} \qquad (15)$$

From eq. (15) we have $\sqrt{6/21}$ for the GT and $\sqrt{15/21}$ for the F weights, respectively. The matrix elements weighted in this way are $M\,'^{DCE}_T(GT) = 0.22$ and $M\,'^{DCE}_T(F) = 0.24$. Consequently, we could infer the matrix element for the $0\nu\beta\beta$ decay of ^{40}Ca

$$M(0\nu\beta\beta;\ ^{40}\text{Ca}) = [(g_v/g_a)^2 M\,'^{DCE}(F) + M\,'^{DCE}(GT)] = 0.62 \cdot 0.24 + 0.22 = 0.37 \pm 0.18 \qquad (16)$$

where $g_{a,v}$ are the axial and vector coupling constants of the weak interaction, respectively [4]. This small number reflects the Pauli blocking, as discussed in Section 6.1.

In the analysis presented so far we have considered pure F of GT transitions. Since the used volume integrals of the nucleon-nucleon refer to the spin and isospin degrees of freedom (not depending on the multipolarity) they can be used also for forbidden transitions. The multipole distribution is accounted for in the sum over the intermediate states, contained in the G propagator (eq. (7)). A possible way to approximate this sum when many multipolarities are present is to replace the energy of the intermediate states by an average value and the sum over intermediate states by closure $\sum_n |n\rangle\langle n| = 1$. Following this approximation we found that the GT-like and F-like NMEs change of 20% (within our quoted uncertainty) for average energy ranging between 0 and 50 MeV.

To speculate, a comparison between the present result for ^{40}Ca and the NME of $0\nu\beta\beta$ decay of ^{48}Ca can be done assuming pure F anf GT and artificially removing the effect of the Pauli blocking, since the same single particle shells are involved but no Pauli blocking is active in the ^{48}Ca case. This is possible by just multiplying M($0\nu\beta\beta$; ^{40}Ca) · 7 = 2.6 ± 1.3. It is noteworthy that this number is compatible with literature for the calculations of the ^{48}Ca $0\nu\beta\beta$ NME [3], [10].

Scientific achievements

In conclusion, this work shows for the first time high resolution and statistically significant experimental data on heavy-ion double charge exchange reactions in a wide range of transferred momenta. The measured cross-section angular distribution shows a clear oscillating pattern, remarkably described by an $L = 0$ Bessel function, indicating that a simple mechanism is dominant in the DCE reaction. This is confirmed by the observed suppression of the multi-nucleon transfer routes.

Strengths factors and matrix elements are extracted under the hypothesis of a two-step charge exchange process. Despite the approximations used in our model, which determine an uncertainty

of ±50%, the present results are compatible with the values known from literature, signaling that the main physics content has been kept. The DCE unit cross section is likely to be a predictable quantity, in analogy to the CE processes. We believe that this finding is mainly due to the particularly simple transitions which take place in the $^{18}O \rightarrow {}^{18}F \rightarrow {}^{18}Ne$, characterized by a strong dominance of single 1^+ and 0^+ ^{18}F states in both *GT* and *F* transitions, respectively. This makes the $(^{18}O,^{18}Ne)$ reaction very interesting to investigate the DCE response of the nuclei involved in *0νββ* research.

A deeper investigation of DCE reactions is worthwhile in the future, studying other systems and different bombarding energies, in order to explore the systematic behavior. A rigorous treatment of the full reaction process in a quanto-mechanichal framework will be the next step toward a more accurate determination of *0νββ* NMEs.

Phase2: Toward "hot" cases

From the pilot experiment toward the "hot" cases

The results discussed above indicate that suitable information from heavy-ion induced DCE reactions can be extracted. In particular the determination of nuclear matrix elements for these processes seems to be at our reach. As a consequence precious information for $0\nu\beta\beta$ matrix elements can be extracted. The availability of the MAGNEX spectrometer for high resolution measurements of very suppressed reaction channels was essential for such a pioneering measurement. However with the present set-up it is difficult to suitably extend this research to the "hot" cases, where $\beta\beta$ decay studies are and will be concentrated. We consider that:

a) About one order of magnitude more yield would have been necessary for the reaction studied, especially at backward angles where large amounts of linear momentum (1-2 fm^{-1}) are available;

b) The (^{18}O,^{18}Ne) reaction is particularly advantageous, due to the large value of both the B[GT;^{18}O$_{gs}$(0$^+$)$\rightarrow$ ^{18}F$_{gs}$(1$^+$)] and B[GT;^{18}F$_{gs}$(1$^+$)$\rightarrow$ ^{18}Ne$_{gs}$(0$^+$)] strengths and to the concentration of the GT strength in the ^{18}F(1$^+$) ground state. However this reaction is of $\beta^+\beta^+$ kind, while most of the research on $0\nu\beta\beta$ is on the opposite side;

c) None of the reactions of $\beta^-\beta^-$ kind looks like as favorable as the (^{18}O,^{18}Ne). For example the (^{18}Ne,^{18}O) requires a radioactive beam, which cannot be available with comparable intensity. The proposed (^{20}Ne,^{20}O) or the (^{12}C,^{12}Be) have smaller B(GT), so a sensible reduction of the yield is foreseen in these cases;

d) In some cases gas target will be necessary, e.g. ^{136}Xe or ^{130}Xe, which are normally much thinner than solid state ones, with a consequent reduction of the collected yield;

e) In some cases the energy resolution we can provide (about half MeV) is not enough to separate the ground state from the excited states in the final nucleus. In these cases the coincident detection of γ-rays from the de-excitation of the populated states is necessary, but at the price of the collected yield.

f) A strong fragmentation of the double GT strength is known in the nuclei of interest compared to the ^{40}Ca.

Taking these considerations into account we realize that the present limit of low beam current we have experienced both for the CS accelerator and for the MAGNEX focal plane detector must be sensibly overcome. For a systematic study of the many "hot" cases of $\beta\beta$ decays an upgraded set-up, able to work with two orders of magnitude more current than the present, is thus necessary. This goal can be achieved by a substantial change in the technologies used in the beam extraction and in the detection of the ejectiles. For the accelerator the use of a stripper induced extraction is an adequate choice. More details about that are in the technical part of this project. For the spectrometer the main foreseen upgrades are:

1. The substitution of the present FPD gas tracker with a GEM tracker system;

2. The substitution of the wall of silicon pad stopping detectors with SiC detectors or similar;
3. The enhancement of the maximum magnetic rigidity;
4. The introduction of an array of detectors for measuring the coincident γ-rays.

Experimental activity

The feasibility of DCE measurements at INFN-LNS with MAGNEX spectrometer, using the CS beams, was already demonstrated as explained before. To use this precious know-how for future application of this methodology to the relevant reaction of interest in the $0\nu\beta\beta$ search, we need to go through a Phase2. During the Phase2 the necessary work for the upgrading of both the accelerator and MAGNEX will be carried out still preserving the access to the present facility. Due to the relevant technological challenges connected the Phase2 is foreseen to have a duration of about 3-4 years. In the meanwhile, experiments with integrated charge of tens of mC (about one order of magnitude more than collected in the pilot experiment) will be performed. These will require several weeks (4-8 depending on the case) data taking for each reaction, since thin targets (a few 10^{18} atoms/cm^2) are mandatory in order to achieve enough energy and angular resolution in the energy spectra and angular distributions. The attention will be focused on a few favorable cases, as discussed below, with the goal to achieve conclusive results for them.

The Phase2 is crucial to allow us to optimize the experimental conditions and open a new challenging research field, carrying out an experimental investigation of few candidate nuclei for the $\beta\beta$ decay. In this framework, we propose to study the (^{18}O,^{18}Ne) reaction as a probe for the $\beta^+\beta^+$ transitions and the (^{20}Ne,^{20}O), or alternatively the (^{12}C,^{12}Be), for the $\beta^-\beta^-$, with the aim

1. to explore the DCE mechanism in both directions, to assure that the extracted NME for the ground-to-ground transitions are compatible;

2. to find the best compromise between energy resolution and count rate for the selected nuclei;

3. to map different combination of scalar and vector nucleon-nucleon interaction by changing the beam energy.

4. To look for the best kinematical conditions in which the direct DCE cross section is dominant respect to the competing multi-step channels cross sections;

5. to probe the dependence of the cross section on the linear momentum transfer;

6. to check the predicted difference among the nuclei in which protons and neutrons occupy the same major shells and those in which they occupy different ones. The magnitude of the Fermi matrix element, which is related to the overlap of the proton and neutron wave functions, is different in these two classes of nuclei, being large in the former and small in the latter case.

21

We select two systems, one for each of the above mentioned two classes of nuclei: the ^{76}Ge-^{76}Se pair for the first class and the ^{116}Cd-^{116}Sn pair for the second. For these nuclei the ground states are resolvable from excited states by MAGNEX (being respectively 562 keV for ^{76}Ge, 559 for the ^{76}Se, 1.29 MeV for ^{116}Sn and 513 for ^{116}Cd) and the production technologies of the thin targets are already available at LNS. We also plan to explore also ^{130}Te and ^{106}Cd [60], that are candidates for $0\nu\beta\beta$ already at our reach in terms of energy resolution and availability of thin targets.

In detail we propose to perform the experiments listed in Table 1 during NUMEN Phase 2, with the aim to investigate the best working conditions for the experimental campaign. For each of them, the complete net of reactions involving the multi-step transfer processes, characterized by the same initial and final nuclei, as it is shown in Fig.4, will be studied under the same experimental conditions.

Table 1.Time table for NUMEN Phase 2 experiments

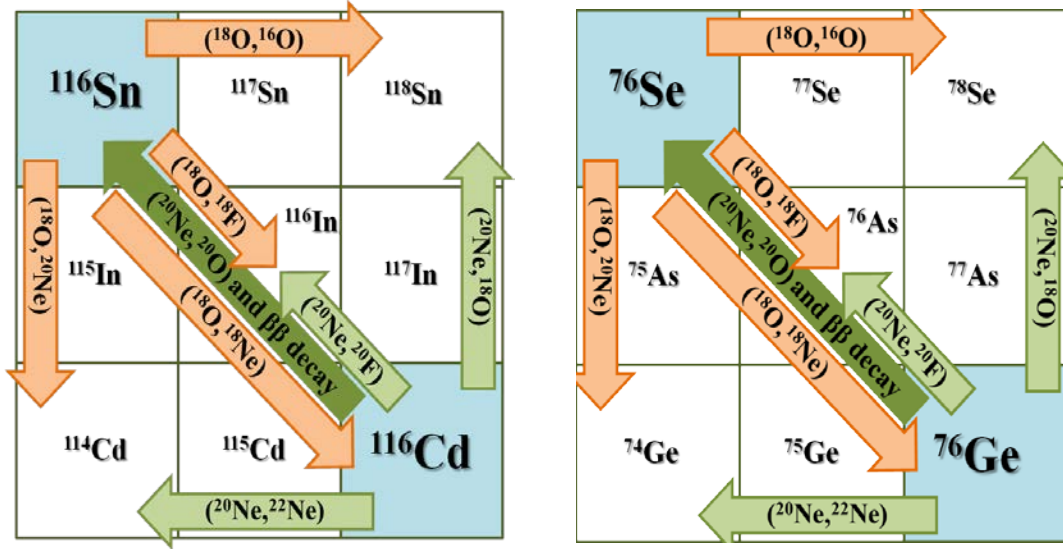| Reaction	Energy (MeV/u)	2016				2017				2018			
			I	II	V		I	II	V		I	II	V
^{116}Sn (^{18}O,^{18}Ne) ^{116}Cd	15-30	■	■										
^{116}Cd (^{20}Ne,^{20}O) ^{116}Sn	15-25			■	■								
^{130}Te (^{20}Ne,^{20}O) ^{130}Xe	15-25					■	■						
^{76}Ge (^{20}Ne,^{20}O) ^{76}Se	15-25							■	■				
^{76}Se (^{18}O,^{18}Ne) ^{76}Ge	15-30									■	■		
^{106}Cd(^{18}O,^{18}Ne) ^{106}Pd	15-30											■	■

Figure 4: Scheme of the complete net of processes that will be studied in the case of the ^{116}Cd – ^{116}Sn and ^{76}Ge – ^{76}Se pairs of nuclei of interest for the $\beta\beta$ decay. Inside the arrows the reaction used to populate the final nuclei is indicated.

During the Phase2 the data reduction strategy will be optimized and the link with the theoretical physics will be strengthen, especially in the view of the construction of a "universal" framework, where $\beta\beta$-decay and DCE reactions are coherently analyzed.

The completion of the experimental activity of NUMEN Phase2 would represent by itself a ground-breaking result, looking forward the main goal of the proposal that has the ambition to indicate a new generation of experiments, with the challenging perspective, in the long term, to provide key information to the community to go deep insight the true nature of neutrino.

R&D and MAGNEX upgrade and Theoretical developments

As mentioned above a manifold upgrade of the MAGNEX spectrometer is mandatory in order to cope with the challenging experimental conditions foreseen by the NUMEN project. In the following an overview of the main items is presented and the time evolution sketched in Table 2.

i. A new gas tracker

The first direct consequence of the increase of the beam current is the need of a specially tailored tracker at the MAGNEX focal plane. The present FPD gas tracker, based on a series of drift chambers and on the use of long multiplication wires [39] is intrinsically limited to about 1 kHz due to the slow drift of positive ions from the multiplication wires to the Frish grid.
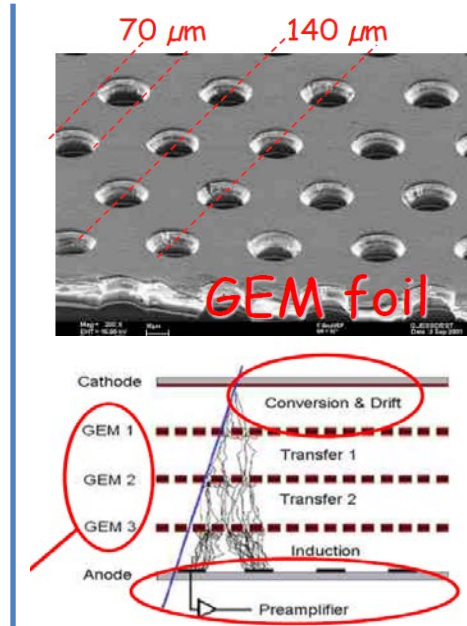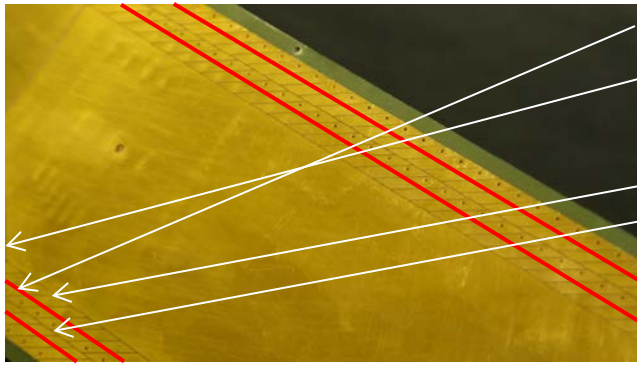
Figure 5: (Left) Front view of the MAGNEX segmented electrode. The red lines are intended to indicate the position of otherwise inviable multiplication wires. The white arrows represent typical ions track. (Right top) Zoomed view of a GEM foil. (Right bottom) Layout of a triple-GEM electron multiplier.

This limit can be overcome substituting the multiplication wires with a series of GEM foils, without changing the geometry of the drift sections of the detector (see Fig. 5). The GEM technology in fact is extremely fast since the primary electrons are multiplied in a series of many independent holes and since the Frish grid can be mounted very close to the GEM planes. In recent developments, detectors based on this technology have been proven to work up to several Mhz/mm^2, i.e much beyond the expected rates in NUMEN. In addition anolog signals, preserving the information of the charge generated by the particle track and the crossing time, can be processed by the read-out of segmented electrodes downstream the GEM foils. This allows to reconstruct with sub-millimetric resolution the tracks of the primary electrons and consequently that of the impinging particles. However large part of the R&D studies on GEM deal with the application at atmospheric pressure and beyond, feature not available for NUMEN, where the ideal working pressure for the spectrometer energy resolution, is about 10 mbar. In addition the GEM are often used at energies where all particle behave as Minimum Ionizing Particles (MIP). In the case foreseen for NUMEN ions with rather different ionizing power will be detected, thus requiring a broad dynamic range (typically larger than 30:1). The development of suitable technologies for the construction of a GEM-based tracker, working at low pressure and wide dynamic range, will be a key issue of the R&D activity during Phase 2.

A specific interest in collaborating on this topics has been manifested by our colleagues of INFN-LNF, whose expertise in GEM detectors is well established. The performance of initial tests of existing 3-foils GEM prototypes were already discussed. The tests will be performed in the

forthcoming weeks. The idea is to insert the prototype inside an existing low pressure chamber and study the positive ion backflow as a functions of the applied voltage for different pressures. These tests will be at the basis of the construction of a suitable prototype detector, which also includes the initial versions of the read-out electronics. Forthcoming tests of the prototype with radioactive sources and heavy-ion beams will be performed afterward at the LNS. The know-how achieved in the first part of the project will be then dedicated to the design of the final detector and read-out electronics. Finally the actual detector will be constructed.

ii.   Ion Identification

NUMEN Phase 2 will also investigate promising technologies for stopping detectors, which need also to be upgraded in view of the high detection rate. Standard technologies, based on silicon pad detectors or plastic scintillators, require a high degree of segmentation (and thus high costs) in order to avoid double-hit events. At the beam currents expected for NUMEN the probability of a double hit at the focal plane is considerable starting for 5 cm^2 area detectors for (^{18}O,^{18}Ne) reaction at 0°. In addition, the radiation hardness of such devices is not enough to avoid a short lifetime of these detectors. For example, in the same reaction (^{18}O,^{18}Ne) the rate limit of about 10^8 ions/cm^2, above which a silicon detector starts to deteriorate is reached in a few days. Interesting opportunities arise from the new technology of SiC crystals, which preserves many of the good properties of silicon detectors, but are much harder to radiation. Improvements in epitaxial SiC growth means that semi-insulating epitaxial SiC layers have recently become available, with thicknesses up to 100 μm. However R&D is still necessary to explore the possibility to build a reliable number of detectors for heavy ions by these epitaxial SiC.

Starting from these consideration we propose to invest resources for R&D in order to explore, characterize and build, after the GEM tracker, a wall of telescopes based on thin epitaxial SiC (100 μm thickness) for energy loss followed by thick (about 1 cm) CsI detectors for residual energy. This solution looks like to be promising because it decouples the GEM tracker from particle identification (PID) function and it is based on existing SiC technology, even if not yet implemented in commercial large area detectors. Test of characterization of epitaxial SiC under heavy ion beams are scheduled next months at the LNS in collaboration with colleagues from CNR. An ad-hoc prototype of an epitaxial SiC detector will be also built and characterized during the next months. After that a SiC-CsI telescope module will be assembled including the basic pieces of the read-out electronics and the PID sensitivity studied under heavy ion beams. The know-how will be then spent to design and construct the final PID-wall for MAGNEX.

iii.   Increase the magnetic rigidity

As mentioned before the MAGNEX spectrometer is a suitable tool for the research foreseen by NUMEN. In fact it guarantees a large solid angle (50 msr) and momentum range (25%) together with a high mass (~ 1/200), momentum (~ 1/2000) and angular (~ 0.2°) resolution. In addition, it can explore a large angular range from 0° to backward angles and can be set, without major changes, to detect particles ranging from protons to medium-mass nuclei, with a very low detection

threshold (hundreds of keV/u). However its maximum magnetic rigidity is limited to about 1.8 Tm, which corresponds to about 50 MeV/u for $^{20}Ne^{10+}$, but less than 30 MeV/u for $^{20}O^{8+}$.

This limit should be reasonably increased in order to explore DCE reactions in the convenient dynamical conditions around 50 MeV/u, where the Gamow-Teller-like modes prevail over the Fermi-like ones. This implies that at least the magnetic rigidity should be raised up to 2.8 Tm, which requires the use of superconducting magnets if the successful optical layout of MAGNEX is to be preserved. A more conservative approach is to work in a slight saturated field with the existing magnets, which allows to reach about 2.1-2.2 Tm, i.e. about 65 MeV/u for $^{20}Ne^{10+}$, 40 MeV/u for $^{20}O^{8+}$. This implies the upgrade of the existing power supplies. Contacts with manufacturers will soon clarify the technical and budgetary impact of this strategy.

iv.   *Exclusive measurements*

An array of scintillators will also be studied within NUMEN Phase2. These detectors are intended for detecting γ-rays from the de-excitation of the residual nucleus (and ejectile) in coincidence with the spectrometer, thus improving the resolution in the energy spectra. In principle this is not part of the spectrometer (as the GEM tracker and the stopping detectors are). However, if we go to 50 MeV/u the energy resolution for heavy ions can be rather poor (1/1000 of 1 GeV ^{18}Ne corresponds to about 1 MeV, or even worse if the beam finite resolution and energy straggling at the target is considered). In this sense the use of an array of detectors for γ-rays is mandatory for DCE reactions. Similarly to the focal plane, the challenge here is to work in a very intense flux of γ-rays and neutrons produced also by the interaction of the beam with the target. This implies a good energy resolution in order to optimize the signal-to-noise ratio and reduce the probability of spurious coincidences. Interesting options as the HPGe, $LaBr_3(Ce)$ or CsI will be studied in detail. The former especially represent a superior solution, despite more expensive. There is, however, an extensive work being done on HPGe and $LaBr_3(Ce)$ by other collaborations that can be used for this purpose. In addition members of the Italian-Brasilian (see INFN-IFUSP-IFUFF collaboration MoU) collaboration are interested to collaborate on this topics with possible in-kind contribution in the future development of NUMEN.

During Phase2 the strategy is to build small prototypes for different detector materials and, after a characterization with radioactive sources, use them under realistic experimental conditions (intense beams, coincidence with MAGNEX, study of DCE) at the LNS. The results of these tests and the consequent choice of the "best" high-flux technology for γ-rays and neutrons will be an important delivery of NUMEN Phase2, which will conduct to the design of the final detector assembly.

Table 2: Time table for NUMEN Phase 2 R&D activity.

R&D item	Activity	2016				2017				2018		
			I	II	V		I	II	V		I	II	V
Ion Tracker	Low pressure tests	red	red										
	Electric field simulations	red	red										
	Study of positive ions backflow	red	red	red									
	Development of read-out system		yellow	yellow	yellow	yellow							
	Construction of a prototype			blue	blue	blue							
	Tests with radioactive-sources and beam					green	green	green	green	green			
	Design of the final detector							purple	purple				
	Design of the final segmented read-out electrode							orange	orange	orange			
	Construction of the final detector										cyan	cyan	cyan
PID-wall	Radiation hardness test of SiC e CsI	red	red	red									
	Prototyping different thicknesses and area SiC detectors		blue	blue	blue								
	Building a SiC-CsI PID module				green	green							
	Developing read-out electronics				orange	orange	orange	orange					

Category	Task	1	2	3	4	5	6	7	8	9	10	11	12
	Design of the final PID-wall						■	■	■				
	Construction of the final detector									■	■	■	■
Magnetic rigidity	Magnetic field simulations	■	■										
	Installation of new power supplies									■	■	■	■
γ-ray calorimeter	Prototyping different detector solutions	■	■										
	Radio-active source and in-beam tests			■	■	■	■	■					
	Design of the final detector assembly							■	■	■	■		
								■	■	■	■		

v. *Electronics: front-end and read out*

The objective of the research and development activities, regarding the upgrade of the focal plane detector (FPD) and the γ wall detectors of NUMEN, is the design and the construction of different prototypes of electronics boards which will act as a test platform for the prototype detectors.

The preliminary study for the design and construction of the final electronics consists in:

a) Front-end board for the pre-amplification, the shaping and subsequent digitization of signals from FPD trackers, designed to be compliant with the for the high event rate and level of exposure to radiations foreseen in the final conditions;

With this aim, a front-end ASIC, the VMM2 chip, identified among those documented in the literature and available in the next years, will be acquired. The VMM2 chip is a strong candidate as the front-end of all the types of detectors in FPD, thanks to the high flexibility of its working parameters. Contacts with the research group of Prof. Gianluigi De Geronimo, (Head of Microelectronics - Instrumentation Division at Brookhaven National Laboratory, NY, USA), who

developed the VMM2 chip, have been started in order to evaluate the implementation of VMM2 or VMM3 for NUMEN.

A hosting board for the VMM2 chip will be designed and constructed. In this way it will be possible to characterize the response of the chip stand alone, for its characterization, and in connection with the first prototypes of trackers available. The trigger and calibration strategies, the interface to the temperature and power supply control systems and the mechanical support, will be tested.

A new version of the chip, the VMM3, is now under design. We will follow the development of this device in order to evaluate if it matchs the specific requirements of the FPD front-end. To this purpose specific tests are planned.

b) Front-end board for the digitization and acquisition of signals from the photosensors employed to read-out the scintillation light of the gamma wall detector.

The plan is to employ for this purpose a chip designed and manufactured by PSI, the DRS3 chip, which allows the fast and low power analog sampling and multiplexing.

The evaluation board for the DRS3 chip will be acquired and a board for the interface to the sensors and to DAQ will be designed.

As in the previous case, the trigger and calibration strategies, the interface to sensors, the mechanical support and temperature and power supply control systems will be tested.

c) Read-out board for the digitization / capture of the front-end signals.

These boards will be based on last generation System On Module (SOM) and programmable logic (FPGA) and ensure an appropriate data bandwidth towards mass storage as well as the total re-configurability and flexibility through the powerful multi-level programming, firmware and software, that characterizes these systems.

The architecture, both hardware and software, is designed modular and scalable and the intelligence on board will allow for great flexibility in the overall data acquisition strategy, i.e. the trigger, the zero suppression, the data communication protocols and the slow control.

In the first phase, it will be sufficient the construction, the test and the validation of each modular element ensuring, at the same time, that the built systems already exhibit the characteristics needed for the interconnections and the integration of the final system.

The possibility of using existing systems designed for similar applications or matching the specifications in our project has been analyzed.

As the first prototypes become available, a measurement and characterization campaign is foreseen, both locally, at the Department of Physics and Astronomy and the LNS, both in specialized laboratories at Brookhaven and CERN.

vi.   Data Handling

The NUMEN data rate to be written on disk is estimated to be between 20 MB/s and 200 MB/s, depending on the beam configuration and on the trigger settings. Such a rate can be handled (i.e. written on disk) by commercial solutions, readily available on the market.

The SOM modules of the electronics provide a data stream already formatted according to the TCP/IP standard protocol and transmitted over a standard Ethernet cable. One network switch (10 Gbit/s uplink) is used to collect and route the Ethernet cables coming from the SOMs. Depending on the number of cables coming from the SOMs and on the individual data rate, an additional switch could be necessary.

The key component of the system, which suits all requirement and which is easily found on the market, is a one- or two-CPU 32-core server, equipped with two 10 Gbit/s Ethernet cards. Only a small fraction of the cores will be busy with the disk writing. Therefore, the free cores can be used for the event building (i.e. match the information of the same events coming from the different detector systems through different data streams) and/or for other online processing. The online processing could potentially reduce the amount of data written on disk (e.g. by compression), thus saving on the storage costs.

An additional small server can be included to handle in a transparent way the run control and the slow control, including the detector settings and interaction with the SOMs. Alternatively, the free cores of the main server (or the free CPU) could be used for the slow control and for the run control. A backup server, which is ideally a clone of the main server, both as hardware and as software, is also foreseen; the backup server can be immediately replace the main server and set to work, in case of a failure of the main machine during the data taking. The spare server could be also used for offline data processing.

The interface to the storage component is a RAID6 Fibre Channel controller, which can write on disk up to 16 Gbit/s (= 2 GB/s). The targeted dimension for the RAID6 disk storage is about 0.5 PB. Racks with such a capacity are commercially available. Since NUMEN will be intrinsically made by many independent runs, with different target nuclei, an alternative solution is to have a partitioned storage (e.g. blocks of 48x1.5" 4 TB disks, totaling 160 net TB each).

A schematic conceptual layout of the acquisition and storage system is displayed below:
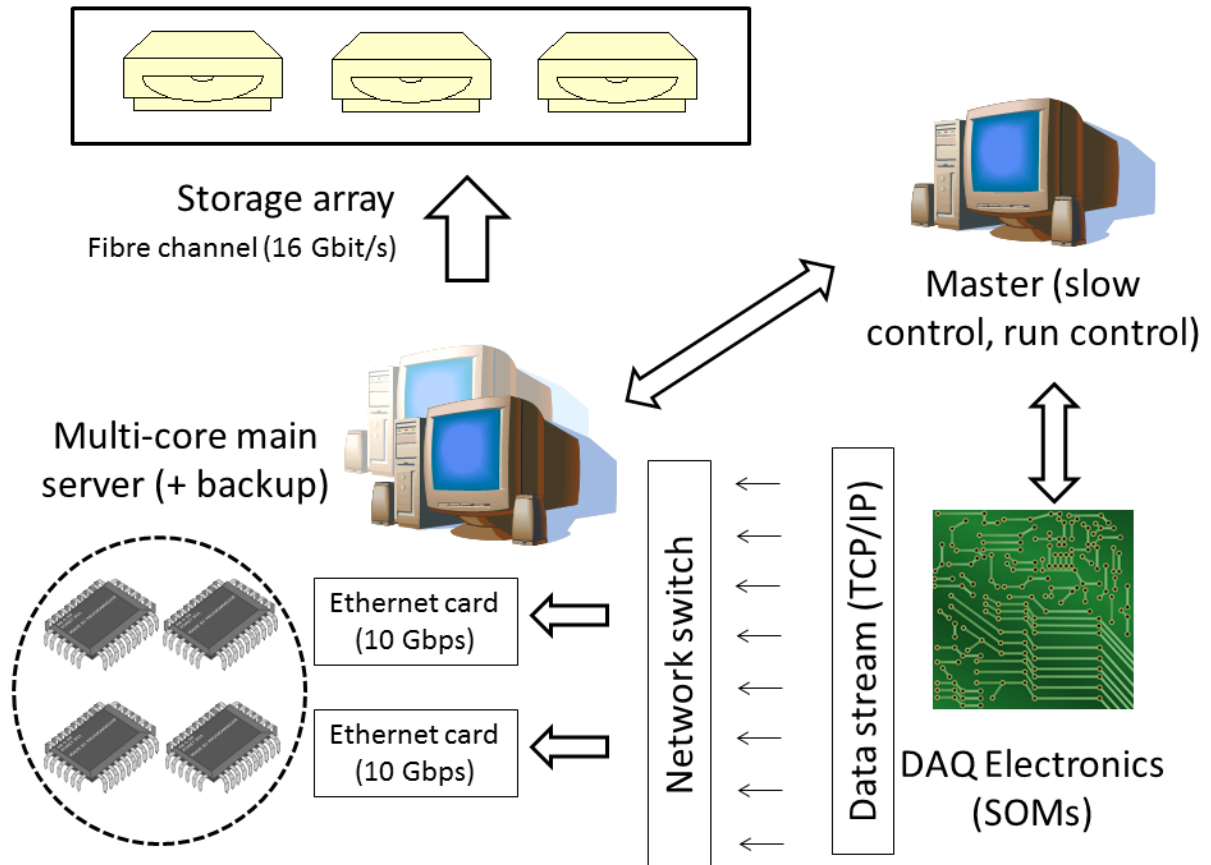
The entire system must be equipped with the appropriate support infrastructure (e.g. cooling, UPS), to be designed and implemented in collaboration with the IT Service on LNS. Furthermore, all data written on disk will be backed-up on magnetic tapes (LTO-6 cartridges). The anticipated data rate does not allow for a backup in real time during the data taking with the beam, so backup sessions will be performed in double copy immediately after the end of each measurement, so to minimize the risk of data losses.

vii.   *Theoretical developments*

The theory program, which will be developed in the framework of the DWBA theory, will follow the steps outlined below. We plan to:

a) Improve, already at the analytical level, the theoretical description of double charge exchange reactions, to get a deeper insight into the reaction mechanism and the essential ingredients ruling the process.

b) Model double charge exchange reactions, employing several approaches (QRPA, shell model, IBM) for inputs connected to nuclear structure quantities.

c) Compare the theoretical predictions to the NUMEN experimental data. This step will allow one to test the ingredients and the approximations adopted in the different approaches, and to identify the experimental conditions which are more suitable to extract, by this comparison, the nuclear matrix elements of the double charge exchange process.

31

d) Investigate the analogy between the theoretical description of the neutrino-less double beta decay, and of double charge exchange reactions. Then, on the basis of the results of point c), we expect to get an insight into the possible link between the different terms that contribute to the nuclear matrix element of the double beta decay and the nuclear matrix elements extracted from the study of double charge exchange reactions. The development of this program will benefit of the collaboration with the major experts in the field of nuclear reaction theory.

Phase3: The facility upgrade

Once all the building block for the upgrade of the accelerator and spectrometer facility will be ready at the LNS a Phase3, connected to the disassembling of the old set-up and re-assembling of the new will start. An estimate of about 18-24 months is considered. During this period the group will be devoted to the data analyses, to the preparation of the next experiments and test of the new detectors with Tandem beams. In addition, if necessary, experiments on single charge exchange or transfer reactions will be performed in other laboratories in order to provide possible pieces of information still lacking, e.g. measurements of B(GT) or transfer amplitudes.

Phase4: The experimental campaign

To perform the experimental campaign that we propose it is necessary the CS upgrade to give high beam intensity and the upgrade of the detection system. Actually, we require a new focal plane detector, suitable to resist to high rates, and a modular gamma detector system that, together, allows us to complete the last phase of measurements, spanning among all the nuclei of interest for our studies. The Phase4 will consist of a series of experimental campaigns at high beam intensities (some pμA) and long experimental runs in order to reach in each experiment integrated charge of hundreds of mC up to C, for the experiments in coincidences, spanning all the variety of candidate isotopes, like:

^{48}Ca, ^{82}Se, ^{96}Zr, ^{100}Mo, ^{110}Pd, ^{124}Sn, ^{128}Te, ^{130}Te, ^{136}Xe, ^{148}Nd, ^{150}Nd, ^{154}Sm, ^{160}Gd, ^{198}Pt.

Actually, once selected the optimal experimental condition for the different cases in the Phase2, with the aforementioned upgrades, the Phase4 will be devoted to collect data addressed to give, with an accurate analysis, a rigorous determination of the absolute cross sections values and their uncertainties for all the system of interest, to the challenging determination of the $0\nu\beta\beta$ decay nuclear matrix elements, that is the ambitious goal of the present proposal.

References

E. Caurier, J.Menendez, F. Nowacki, A. Poves, Phys. Rev. Lett. 100 (2008) 052503.

1]

J. Suhonen and M.Kortelainen, Int. Journ. of Mod. Phys. E 17 (2008) 1.

2]

N. L. Vaquero, T.R. Rodriguez, J. L.Egido, Phys. Rev. Lett. 111 (2013) 142501.

3]

J. Barea, J. Kotila, F. Iachello, Phys. Rev. C 87 (2013) 014315.

4]

H. Akimune, et al., Phys. Lett. B 394 (1997) 23.

5]

J. P. Schiffer, et al., Phys. Rev. lett. 100 (2008) 112501.

6]

D. Frekers, Prog. Part. Nucl. Phys. 64 (2010) 281.

7]

C.J. Guess, et al., Phys. Rev. C 83 (2011) 064318.

8]

S. J. Freeman and J. P. Schiffer, J. Phys. G: Nucl. Part. Phys. 39 (2012) 124004.

9]

J. Barea, J. Kotila and F. Iachello, Phys. Rev. Lett. 109 (2012) 042501.

10]

Report to the Nuclear Science Advisory Committee, Neutrinoless Double Beta Decay, 2014.

11]

J.D. Vergados, Phys. Rev. D 25 (1982) 914.

12]

A. Fazely and L. C. Liu, Phys. Rev. Lett. 57 (1986) 968.

13]

S. Mordechai, et al., Phys. Rev. Lett. 61 (1988) 531.

14]

N. Auerbach, et al., Ann. Phys. 192 (1989) 77.

15]

J. Blomgren, et al., Phys. Lett. B 362 (1995) 34.

16]

F. Naulin, et al., Phys. Rev. C 25 (1982) 1074.

17]

D. M. Drake, et al., Phys. Rev. Lett. 45 (1980) 1765.

18]

D.R. Bes, O. Dragun, E.E. Maqueda, Nucl. Phys. A 405 (1983) 313.

19]

20]   C.H. Dasso, A. Vitturi, Phys. Rev. C 34 (1986) 743.

21]   W. von Oertzen, et al., Nucl. Phys. A 588 (1995) 129c.

22]   H. Matsubara, et al., Few-Body Systems 54 (2013) 1433.

23]   D. M. Brink, Phys. Lett. B 40 (1972) 37.

24]   P. Puppe, et al., Phys. Rev. C 84 (2011) 051305.

25]   W.P. Alford and B.M. Spicer, Advances in Nucl. Phys. 24 (1998) 1.

26]   J. Menéndez, D. Gazit, A. Schwenk, Phys. Rev. Lett. 107 (2011) 062501.

27]   L. Mandelstam and Ig. Tamm, J. Phys. USSR 9 (1945) 249.

28]   T. N. Taddeucci et al. Phys. Rev. C 28 (1983) 2511.

29]   T.N. Taddeucci et al. Nucl. Phys. A469 (1987) 125.

30]   F. Osterfeld, Rev. of Mod. Phys. 64 (1992) 491.

31]   D. Frekers, et al., Nucl. Phys. A 916 (2013) 219.

32]   Y. Fujita, B. Rubio, W. Gelletly, Progress in Particle and Nuclear Physics 66 (2011) 549.

33]   C. Baumer, et al., Phys. Rev. C 71 (2005) 024603.

34]   A. Negret, et al., J. Phys. G: Nucl. Part. Phys. 31 (2005) 1931.

35]   F. Cappuzzello et al., Nuclear Physics A 739 (2004) 30.

36]   G. R. Satchler, Direct Nuclear reactions, Oxford Science Publications, 1983.

37]   Ph. Chomaz, N. Frascaria, Phys. Reports 252 (1995) 275.

38]   F. Cappuzzello et al., MAGNEX: an innovative large acceptance spectrometer for nuclear reaction studies in: Magnets: Types, Uses and Safety, Nova Publisher Inc., New York, 2011, pp 1-63.

39]   M. Cavallaro, et al., Eur. Phys. J. A (2012) 48: 59.

40]   D. Carbone, et al., Eur. Phys. J. A (2012) 48: 60.

41]   M. Bondì, et al., AIP Conf. Proc. 1595 (2014) 245.

42]   F. Cappuzzello, et al., Nucl. Instr. and Meth. A 621 (2010) 419.

43]   M. Cavallaro, et al., Nucl. Inst. and Meth. A 648 (2011) 46.

44]   F. Cappuzzello, et al., Nucl. Instr. and Meth. A 638 (2011) 74.

45]   M. Cavallaro, et al., Nucl. Instr. and Meth. A 637 (2011) 77.

46]   F. Cappuzzello, et al., Nucl. Instr. and Meth. A 763 (2014) 314.

47]   F. Ajzenberg-Selove, et al., Phys. Rev. C 32 (1985) 756.

48]   D. R. Tilley, et al., Nucl. Phys. A 595 (1995) 1.

49]   J. A. Cameron and B. Singh, Nucl. Data Sheets 109 (2008) 1.

50]   F. Hofmann and H. Lenske, Phys. Rev. C 57 (1998) 2281.

       Y. Fujita private communication.

51]

M. Matsuo, Phys. Rev. C 73 (2006) 044309.

52]

D.J.Mercer et al. Phys. Rev. C 49 (1994) 3104.

53]

D. E. Alburger and D. H. Wilkinson, Phys. Lett. B 32 (1970) 190.

54]

M. Bhattacharya, C.D. Goodman and A. Garcia, Phys. Rev. C 80 (2009) 055501.

55]

T. Chittrakarn et al., Phys. Rev. C 34 (1986) 80.

56]

B. K. Park, et al., Phys. Rev. C 45 (1992) 1791.

57]

W. Tornow, et al., Phys. Rev. C 42 (1990) 693.

58]

S. Adachi, et al., Nucl. Phys. A 438 (1985) 1.

59]

J. Barea, J. Kotila and F. Iachello Phys. Rev. C 87 (2013) 057301.

60]

S.T. Petcov, Adv. High Energy Phys. 2013 (2013) 852987.

61]

A. Gouvea, P. Vogel, Prog. Part. Nucl. Phys. 71 (2013) 75.

62]

J.D. Vergados, H.E. Ejiri, F. Simokovic, Rep. Prog. Phys. 75 (2012) 106301.

63]

J. Suhonen, O. Civitarese, J. Phys. G 39 (2012) 124005.

64]

S. F. King, Rep. Prog. Phys. 67 (2004) 107.

65]

E. Caurier, J.Menendez, F. Nowacki, A Poves, Phys. Rev. Lett. 100 (2008) 052503.

66]

[67] Nuria Lopez Vaquero, Tomas R. Rodriguez, J. Luis Egido, Phys.Rev.Lett. 111 (2013) 142501.

[68] J. Barea, J. Kotila, F. Iachello, Phys.Rev. C87 (2013) 014315.

[69] F.Simkovic, A Faessler, V.Rodin, P.Vogel, J.Engel, Phys. Rev. C 77 (2008) 045503.

[70] D.R.Bes, O. Dragun, E.E. Maqueda, Nucl. Phys. A 405 (1983) 313.

[71] C.H.Dasso, A. Vitturi, Phys. Rev. C 34 (1986) 743.

[72] T.N. Taddeucci et al. Nucl. Phys. A469 (1987) 125-172.

[73] W.P. Alford and B.M. Spicer, Advances in Nucl. Phys. 24 (1998) 1-82.

[74] F. Osterfeld, Rev. of Mod. Phys. 64 (1992) 491-557.

[75] F. Cappuzzello et al., Nuclear Physics A 739 (2004) 30–56.

[76] F. Cappuzzello et al., Nucl. Instr. and Meth. A 621 (2010) 419–423.

[77] F. Cappuzzello, D. Carbone and M. Cavallaro, Nucl. Instr. and Meth. A 638 (2011) 74–82.

[78] M. Cavallaro et al., Nucl. Instr. and Meth. A 637 (2011) 77–87.

[79] M. Cavallaro et al., Eur. Phys. J. A (2012) 48: 59.

[80] M. Cavallaro et al., Nucl. Inst. and Meth. A 648 (2011) 46.

[81] B.K. Park et al., Phys. Rev. C 45 (1994) 1791.

[82] S. Adachi et al., Nucl. Phys. A 438 (1985) 1.

[83] T.R. Rodriguez, G. Martinez-Pinedo, Phys. Lett. B 719 (2013) 174.

[84] Y. Fujita private communication..

[85] P. Vogel, M. Ericson and J.D.Vergados, Phys. Lett. B 212 (1988) 259.

[86] J.R.B. Oliveira, J. Phys. G: Nucl. Part. Phys. 40 (2013) 105101.

[87] D. Pereira, et al., Phys. Lett. B 710 (2012) 426.

[88] W. von Oertzen, Nucl. Phys. A 482 (1988) 357c.